# Predictability of Ultralong Waves in Global and Hemispheric Quasi-Geostrophic Barotropic Models

JOHN O. ROADS AND RICHARD C. J. SOMERVILLE

*Climate Research Group, Scripps Institution of Oceanography, University of California, San Diego, La Jolla 92093*

(Manuscript received 7 April 1981, in final form 3 November 1981)

ABSTRACT

A global quasi-geostrophic barotropic model, including orography, zonal forcing and frictional dissipation, is compared to two hemispheric models, one with antisymmetric equatorial boundary conditions and one with symmetric boundary conditions. The stationary solutions in the global model and the hemispheric models are found to be different, because the hemispheric models lack either the symmetric or antisymmetric waves, and because the nonlinear feedbacks are much larger in the hemispheric models. Time-dependent calculations show that the hemispheric models can excite anomalous Rossby waves and can produce erroneous short-range forecasts in middle latitudes. We conclude that global models are preferred for making both short-range and long-range forecasts for middle latitudes.

## 1. Introduction

In an ensemble of five-day numerical weather prediction experiments, Somerville (1980) found that the ultralong waves in middle latitudes were forecast markedly less skillfully by a hemispheric model than by a global model. When the initial states in the hemispheric integrations were modified by using a smooth field in the tropics in place of analyzed observed data, the forecasts were still less skillful and the effects were apparent earlier in the five-day period. These experiments, which were carried out using real data and a primitive-equation model, appeared to provide a partial explanation for the low skill of many typical present-day ultralong wave forecasts with hemispheric models, relative to the skill expected from predictability theory. The results also suggested that some improvement in operational forecasting of planetary waves might be expected whenever hemispheric models with poor tropical initial states were replaced by global models initialized with good global data.

The detailed mechanisms by which hemispheric models tend to damage forecasts of ultralong waves were not revealed by these experiments. The errors seemed to be "associated with the spurious excitation of large-amplitude external modes," but it was not clear how these modes came to be excited. The effects were confined mainly to the ultralong waves (zonal wavenumbers 1–3), and the reason for this result was unknown. An unexplained strong variation between cases in the ensemble was also apparent, with some cases being much more sensitive to hemispheric effects than others. This case-dependence provided a possible reason why the effects discovered by Somerville were substantially larger than had been found by earlier research, which had been confined to a small number of cases (e.g., Baumhefner, 1971; Miyakoda and Umscheid, 1973). Also, the speed with which middle latitudes were affected by what appeared to be tropical and interhemispheric phenomena was largely unanticipated and suggested that serious defects might be present in the technology of hemispheric numerical weather prediction. The exact nature of these defects remained a mystery; there was no satisfying theoretical explanation for Somerville's experimental results.

In the present paper, we attempt to show that the results of these numerical experiments can be understood within a very simple conceptual framework, that of quasi-geostrophic dynamics of a quasi-linear barotropic atmosphere. Evidence for the validity of these idealizations has been provided by Lambert and Merilees (1978) and Daley *et al.* (1981). We first construct a global model subject not only to this theoretical constraint, but also to severe spectral truncation. Such simplifications provide tractability and insight. Their adequacy can be judged *a posteriori*. Our model includes orography and an extremely simple form of forcing and frictional dissipation. We next explore the stationary solutions which dominate the "climate" of this model. We find that these solutions differ from those of two hemispheric versions of the model, one with a symmetry condition at the equator and one with an antisymmetry condition. This difference occurs because the hemispheric models lack the complete set of modes of the global model and they display stronger non-

0022-4928/82/040745-11$06.75

linear feedbacks. When time dependence is added, we find that spurious transient Rossby waves are excited in the "weather" of the hemispheric models.

Instead of performing prediction experiments with real data in the manner of Somerville, we have taken advantage of the extreme simplicity of our model to create artificial initial states for it. By constructing these initial states using the known differences between the model structure and resonance properties of the global and hemispheric models, we can sometimes anticipate the manner in which each hemispheric model will or will not be adequate to the task of emulating the performance of the global model for a given initial state. Our simple theoretical model may help us to understand the superiority of the global model in the real-data primitive-equation experiments of Somerville. Of course, a global domain is not a panacea, and much research is needed to improve numerical weather prediction models. Current predictions still "generally resemble one another more than the best of them resembles the real atmosphere."

The very simple global and hemispheric models are described in Section 2. The climate solutions for these models are given in Section 3. The weather solutions for these models are given in Section 4. Section 5 contains conclusions.

## 2. Model

The basic system of equations used in this investigation is derived from an energetically consistent quasi-geostrophic system of equations described by Lorenz (1960), supplemented by a term representing forcing and dissipation

$$\frac{\partial}{\partial t}\nabla^2\psi = -J(\psi, \nabla^2\psi + f) - \nabla\cdot f\nabla\chi + g\frac{\partial\rho}{\partial p}K\frac{\partial}{\partial z}\nabla^2(\psi_e - \psi),$$

$$\nabla^2\chi + \frac{\partial\omega}{\partial p} = 0,$$

where the symbols have their usual meanings, e.g.,

$$g\frac{\partial\rho}{\partial p}K\frac{\partial}{\partial z}(\nabla^2\psi_e - \nabla^2\psi) = \text{vorticity source and sink},$$

$z$ = altitude, $p$ = pressure, $g$ = gravity, $\rho$ = density, $K$ = vertical diffusion coefficient, $\psi$ = streamfunction for non-divergent flow, $\chi$ = velocity potential for divergent flow, and $f$ = Coriolis parameter = $2\Omega\sin y$. Averaging in the vertical and assuming that the pressure velocity $\omega$ vanishes at the top of the atmosphere, we obtain

$$\frac{\partial}{\partial t}\nabla^2\psi = -J(\psi, \nabla^2\psi + f) - \nabla\cdot f\nabla\chi + k\nabla^2(\psi_e - \psi_s),$$

$$\nabla^2\chi + \frac{\omega_s}{p_s} = 0,$$

where $k = gp_s^{-1}\rho_s C_D|V_s|$, $\psi_s$ = surface streamfunction, $\omega_s$ = surface vertical velocity, $\rho_s$ = surface density, $p_s$ = surface pressure, $C_D$ = drag coefficient, and $|V_s|$ = surface wind speed. All non-subscripted variables now represent the vertically-averaged flow and $\psi_e$ includes the vertically-averaged baroclinic forcing. The geostrophic boundary condition is used to determine $\omega_s$ as

$$\frac{\omega_s}{p_s} = -\frac{\rho_s}{p_s}J(\psi_s, gh),$$

where $h$ = orographic height. Thus, the system of equations becomes

$$\frac{\partial}{\partial t}\nabla^2\psi = -J(\psi, \nabla^2\psi + f) - \nabla\cdot f\nabla\chi + k\nabla^2(\psi_e - \psi),$$

$$\nabla^2\chi = \lambda J(\psi, gh),$$

where $\psi_s$ is assumed to be proportional to $\psi$ and the proportionality constant has been absorbed into $\lambda$ and $k$. Scaling all lengths by the radius of the earth and all times by $(2\Omega)^{-1}$, we write this system dimensionlessly as

$$\left.\begin{aligned}\frac{\partial}{\partial t}\nabla^2\psi &= -J(\psi, \nabla^2\psi + \sin y) \\ &\quad - \nabla\cdot\sin y\nabla\chi + k\nabla^2(\psi_e - \psi) \\ \nabla^2\chi &= \lambda J(\psi, gh)\end{aligned}\right\}, \quad (1)$$

where $k$ = surface friction parameter taken equal to $10^{-3}$, $\lambda$ = constant relating velocity potential to the surface orographical uplift taken equal to 2,

$$J(A, B) = \frac{1}{\cos y}\left\{\frac{\partial A}{\partial x}\frac{\partial B}{\partial y} - \frac{\partial A}{\partial y}\frac{\partial B}{\partial x}\right\},$$

$$\nabla^2 A = \frac{1}{\cos^2 y}\frac{\partial^2 A}{\partial x^2} + \frac{1}{\cos y}\frac{\partial}{\partial y}\cos y\frac{\partial A}{\partial y},$$

$x$ = longitude and $y$ = latitude. (1) may be separated into an equation for the zonal mean (denoted by an overbar) and a deviation from the zonal mean (denoted by a carat). The equation for the zonal mean is

$$\left.\begin{aligned}\frac{\partial}{\partial t}\nabla^2\bar{\psi} &= -\overline{J(\hat{\psi}, \nabla^2\hat{\psi})} - \nabla\cdot\sin y\nabla\bar{\chi} \\ &\quad + k\nabla^2(\bar{\psi}_e - \bar{\psi}) \\ \nabla^2\bar{\chi} &= \lambda\overline{J(\hat{\psi}, g\hat{h})}\end{aligned}\right\}, \quad (2)$$

and the equation for the asymmetric deviation from the zonal mean is

$$\left.\begin{aligned}\frac{\partial}{\partial t}\nabla^2\hat{\psi} &= -J(\hat{\psi}, \nabla^2\bar{\psi} + \sin y) - \widehat{J(\bar{\psi}, \nabla^2\hat{\psi})} \\ &\quad - J(\hat{\psi}, \nabla^2\hat{\psi}) - k\nabla^2\hat{\psi} - \nabla\cdot\sin y\nabla\hat{\chi} \\ \nabla^2\hat{\chi} &= \lambda J(\bar{\psi}, g\hat{h}) + \lambda J(\hat{\psi}, g\bar{h}) + \lambda\widehat{J(\hat{\psi}, g\bar{h})}\end{aligned}\right\}. \quad (3)$$

An expansion in Legendre polynomials, $P_l$, is made for the zonal mean terms

$$\bar{\psi} = \sum_{l=0}^{\infty} \bar{\psi}_l P_l(\sin y),$$

$$\bar{x} = \sum_{l=0}^{\infty} \bar{x}_l P_l(\sin y).$$

The asymmetric quantities can be expanded in associated Legendre polynomials (as will be done later for analytic calculations) but the numerical model uses only a Fourier expansion in longitude, i.e.,

$$\hat{B} = \sum_{n=1}^{\infty} \hat{B}_c \cos nx + \hat{B}_s \sin nx,$$

where

$$0 < x < 2\pi,$$

and the meridional variation is calculated by a grid point method, where the grid extends in equal increments from pole to pole with the actual pole and equator placed a half grid point away from the computational grid. Consistent with an expansion in associated Legendre polynomials, $\hat{\psi} = \hat{\chi} = \hat{h} = 0$ at the poles (polar point information is carried by the mean terms). For the hemispheric models

$$\hat{\psi} = \frac{\partial}{\partial y}\hat{\chi} = \frac{\partial}{\partial y}\hat{h} = \frac{\partial}{\partial y}\bar{h} = 0$$

at the equator for the antisymmetric model, and

$$\frac{\partial}{\partial y}\hat{\psi} = \hat{\chi} = \hat{h} = \frac{\partial}{\partial y}\bar{h} = 0$$

at the equator for the symmetric model.

The orography and the numerical procedure for evaluating the Jacobians at specific grid points were given by Roads (1981). For the calculations to be discussed in this paper, the grid points were placed every 7.5° of latitude.

## 3. Climate solutions

Simple stationary solutions can be derived if the zonal flow is assumed to be solid body rotation, and this zonal flow interacts with only one wave at a time. The stationary solutions to (2) are found by omitting the time dependence and using the orthogonality condition to find the contributions to the first mode $P_1$, which gives rise to the solid body rotation. We also make use of the relationship $\nabla^2 P_l = -l(l+1)P_l$. Hence (2) can be written in the form

$$\bar{F} = \bar{T}, \tag{5}$$

where

$$\bar{F} = 2k(\bar{\psi}_e - \bar{\psi}),$$

the frictional forcing and dissipation and

$$\bar{T} = \frac{\int_{-\pi/2}^{\pi/2} \{-\nabla \cdot \sin y \nabla \bar{\chi}\} P_1(\sin y) \cos y dy}{\int_{-\pi/2}^{\pi/2} P_1^2(\sin y) \cos y dy},$$

the mountain torque. It should be noted here that the stationary solutions for zonal modes not in solid body rotation would also be affected by the vorticity transport. However, for solid body rotation this transport is identically zero (e.g., Baer and Platzman, 1961). The velocity potential $\bar{\chi}$ is calculated from (2) in a similar manner. Only one mode is considered, the second symmetric mode. The constant first symmetric mode is not dynamically significant and only the even modes conserve the symmetry in the model. Thus, to be consistent with our truncation for the streamfunction, we take

$$\bar{\chi} = \bar{\chi}_2 = -\frac{\int_{-\pi/2}^{\pi/2} \lambda \overline{J(\hat{\psi}, g\hat{h})} P_2(\sin y) \cos y dy}{6 \int_{-\pi/2}^{\pi/2} P_2^2(\sin y) \cos y dy}.$$

The asymmetric stream functions are calculated from the stationary part of (3) as a function of the orographic heights, friction and zonal streamfunction.

We expect to find stationary or climate solutions whenever $\bar{F} = \bar{T}$, and, as shown by Roads (1981), we expect to find three solutions for each zonal wavenumber and meridional mode. One occurs for $\bar{\psi} = \bar{\psi}_e$ and two others occur near the resonance points in the system. The resonance points can be found by solving the stationary, linear, asymmetric, inviscid form of (3),

$$\nabla \cdot \sin y \nabla \nabla^{-2}(\lambda J(\bar{\psi}, g\hat{h}) + \lambda J(\hat{\psi}, g\bar{h})) = -J(\bar{\psi}, \nabla^2\hat{\psi}) - J(\hat{\psi}, \nabla^2\bar{\psi} + \sin y),$$

which can be written in schematic form as

$$G(\bar{\psi}) = H(\bar{\psi})\hat{\psi}.$$

Near certain values of $\bar{\psi}$, $H(\bar{\psi}) \to 0$ and $\hat{\psi} \to \infty$, that is, $\hat{\psi}$ becomes resonant. To find these values of the zonal streamfunction we solve the equation

$$0 = -J(\bar{\psi}, \nabla^2\hat{\psi}) - J(\hat{\psi}, \nabla^2\bar{\psi} + \sin y), \tag{6}$$

for $\bar{\psi}$. Let $\hat{\psi}$ be represented by a sum of associated Legendre polynomials

$$\hat{\psi} = \sum_{n=0}^{\infty} \sum_{m=-n}^{n} \hat{\psi}_n^m P_n^m(\sin y) e^{im\lambda}. \tag{7}$$

This orthogonal representation has the following eigenvalue relationship

$$\nabla^2 P_n^m e^{im\lambda} = -n(n+1) P_n^m e^{im\lambda}.$$

Thus substituting (7) into (6) results in

TABLE 1. Resonant values of the zonal streamfunction $\bar{\psi}_1$ for solid-body flow. $n$ denotes the $n$th associated Legendre polynomial. For each value of $n$, the value of the zonal mean streamfunction $\bar{\psi}$ at which resonance occurs is given, followed by a list of resonant waves. Each resonant wave is labeled with a pair of numbers. The first number is the zonal wavenumber $m$. The second number gives the number of zeros in the meridional direction, $n - m$. The speed of the zonal wind (in m $s^{-1}$) at the equator is $\sim$1000 times the value of $\bar{\psi}$. Note that for a specific resonant value of the zonal streamfunction, several zonal wavenumbers are in resonance and that the higher the zonal wavenumber, the fewer the number of zeros in the meridional direction.

| $n$ | $\bar{\psi}$ | Waves | | | | | |
|---|---|---|---|---|---|---|---|
| 2 | −0.250 | 11, | 20 | | | | |
| 3 | −0.100 | 12, | 21, | 30 | | | |
| 4 | −0.0556 | 13, | 22, | 31, | 40 | | |
| 5 | −0.0357 | 14, | 23, | 32, | 41, | 50 | |
| 6 | −0.0250 | 15, | 24, | 33, | 42, | 51, | 60 |
| 7 | −0.0185 | 16, | 25, | 34, | 43, | 52, | 61 |
| 8 | −0.0143 | 17, | 26, | 35, | 44, | 53, | 62 |
| 9 | −0.0114 | | 27, | 36, | 45, | 54, | 63 |
| 10 | −0.00926 | | | 37, | 46, | 55, | 64 |
| 11 | −0.00769 | | | | 47, | 56, | 65 |
| 12 | −0.00649 | | | | | 57, | 66 |

$$0 = -\bar{\psi}_1 n(n+1)\hat{\psi}_n^m + (2\bar{\psi}_1 - 1)\hat{\psi}_n^m ,$$

so that if

$$\bar{\psi}_1 = \frac{1}{-n(n+1)+2},$$

resonance results. The presence of friction in the system prevents $\hat{\psi}_n^m$ from achieving infinite amplitudes; nonetheless, we should expect that near these points $\hat{\psi}_n^m$ will be quite large and hence the mountain torque should also be quite large.

To tabulate the resonant waves for each resonant value of the zonal streamfunction, recall that $P_n^m$ has $n - |m|$ zeroes in its meridional variation between the poles, and only those zonal waves that have $|m| \leq n$ are present. The resonant values of the zonal streamfunction for solid body flow are given in Table 1.

Having found the amplitudes of the first zonal mean modes that give rise to resonance, let us now return to the solution of (5). The stationary solutions for the global model are shown in Fig. 1a at the intersection points of the friction function (the straight lines) and the mountain torque lines (the spectra-like lines). Consider first the mountain torque ($T$) lines. Several well-defined peaks occur near the resonant values calculated for the inviscid model. Also, the $T$ curves tend to cluster around specific values for $\bar{\psi}$, but there is some separation. Part of this separation is due to the presence of the zonal mean orography. Fig. 1b, which has the resonance features calculated without the zonal mean orography, shows this feature. Part of the separation is also due to the friction in the system. Without friction, mountain torque would be zero and there would be an infinite response at the resonance points.

As stated previously, the stationary solutions for this model are found at the intersection points of the friction curves (the straight lines) and the $T$ curves (the spectra-like lines). For a specific wavenumber, there are two solutions near a resonance point and one near the zonal forcing equilibrium. The one near the forcing equilibrium can usually be discounted since it would be unstable in a baroclinic model (Roads, 1980a and 1980b). The one on the super-resonant side of the resonance peak is also unstable (Charney and Devore, 1979). Thus for the parameters in this model, only one stationary solution on the sub-resonant side of the resonance peak is likely to be present for each zonal wavelength and meridional mode. There are, however, a number of resonant solutions possible, depending upon the chosen parameters, if multiple waves are allowed.

It should be noted here that the antisymmetric hemispheric model includes only waves with an odd number of modes between the poles, whereas the symmetric model will include only those waves with an even number of modes between the poles. This fact leads to a substantial difference between the stationary solutions to be found in hemispheric models and those in global models. For example, compare the stationary solutions for the global model depicted in Fig. 1a with those of the antisymmetric hemispheric model shown in Fig. 1c. It is immediately noticeable that the antisymmetric hemispheric model is missing the symmetric torques which are present in the global model. It is also noteworthy that the resonance features for the hemispheric model are much stronger. The reason for this difference is that the hemispheric model assumes that the Southern Hemisphere orography is an exact duplicate of that in the Northern Hemisphere and hence a stronger apparent forcing is present in the hemispheric model.

Thus, hemispheric models have stronger nonlinear feedbacks for the waves that are included, but lack certain resonant waves that may be important for describing a basic stationary state. That is, a number of differences in stationary states will be found between global and hemispheric models. For example, if $\psi_e = -0.03$, a stationary subresonant state is found around $\bar{\psi} = -0.025$ and a resonant combination of 15, 24, 33, 42, 51, 60, will be present in the global model, whereas only the even waves will be present in the symmetric hemispheric model and only the odd waves present in an antisymmetric hemispheric model. As another example, if $\psi_e = -0.035$, the global model would have only the solution near $\bar{\psi}_e = -0.035$, whereas the hemispheric antisymmetric or hemispheric symmetric models would also have anomalous resonant solutions near $\bar{\psi} = -0.025$, together with the differences that would result in the standing waves.

## 4. Weather solutions

### a. *Solid body rotation and stationary wave initialization*

If a given synoptic situation is made up of various global waves of which some are even and some are odd functions about the equator, then, in addition to having poor climate solutions, neither of the hemispheric models is likely to produce a very good short-term forecast. For example, let us consider a case in which a particular antisymmetric wave near resonance has been excited. As will be shown later, this wave will tend to be a persistent feature. Let us suppose now that we have a symmetric hemispheric model that we wish to use to forecast only the evolution in the Northern Hemisphere. As anticipated by Somerville (1980), "the partitioning of the initial conditions among modes is done very differently in the global and the hemispheric versions of the model." That is to say, the antisymmetric wave appears in the symmetric hemispheric model in aliased form as a linear combination of symmetric waves, none of which are near a resonance point, and the symmetric hemispheric model will therefore show anomalous phase speeds. A similar argument can be made for the presence of a global symmetric wave and the use of an antisymmetric model.

To make this argument more concrete, consider a basic synoptic situation which can be described by propagating Rossby waves. That is, let

$$\hat{\psi} = \sum_{n=1}^{N} \sum_{m=-n}^{n} \hat{\psi}_n^m P_n^m(\sin y) e^{im\lambda} e^{i\omega t}$$

and neglect the effects of friction, orography and nonlinearity. Then substitution into (3) results in

$$c = \frac{\omega}{m} = -\frac{\{\bar{\psi}[-n(n+1)+2]-1\}}{n(n+1)},$$

where $c$ is the phase speed of the wave and the period of the waves is $\tau_n = 2\pi/\omega$. The values of $\tau_n$ as a function of $\bar{\psi}$ and $n$ are given in Table 2. The values for $\bar{\psi}_1$ are computed from the resonance formula $\bar{\psi}_l = 1/[-n(n+1)+2]$, derived earlier.

The negative values in Table 2 correspond to eastward-propagating Rossby waves and the positive values correspond to westward-propagating Rossby waves. The symbol $\infty$ refers to non-propagating or stationary Rossby waves. The zonal streamfunction values are the resonant ones shown in Table 1. The table is to be interpreted as follows. For a specific zonal wind, a particular associated Legendre polynomial $P_n^{|m|}$ will have a period $\tau_n$. For any zonal wave, $|m| < n$ is necessary. If a hemispheric model is being used, $n - |m|$ must be odd for the antisymmetric models and even for the symmetric models. For example, for $|m| = 1$ only the $\tau_n$ for $n = 2, 4, 6, 8, 10, \ldots$, are present in the antisymmetric model, whereas only the $\tau_n$ for $n = 1, 3, 5, 7, 9, \ldots$, are present in the symmetric model. The global model includes both sets. For $|m| = 4$, the periods for $n = 4, 6, 8, 10, \ldots$, are present in the symmetric model, and only the periods for $n = 5, 7, 9, \ldots$, are present in the antisymmetric model. Again, the global model includes both sets.

In order to understand the basic features of Table 2, we shall refer to four cases below. Case 1 is initialized with $\bar{\psi}_1 = -0.04$, is forced by $\bar{\psi}_e = -0.045$ and has only one zonal wave, $m = 1$. Case 2 is initialized with $\bar{\psi}_1 = -0.019$, is forced by $\bar{\psi}_e = -0.0250$ and has only one zonal wave, $m = 2$. Case 3 is initialized with $\bar{\psi}_1 = -0.0255$, is forced by $\bar{\psi}_e = -0.03$, and has only one zonal wave, $m = 3$. Case 4 is initialized with $\bar{\psi}_1 = -0.0250$, is forced by $\bar{\psi}_e = -0.0375$ and has only one zonal wave, $m = 4$.

The global model initializes the perturbation quantities by solving the stationary form of (3) to find the linear stationary wave associated with the initial zonal stream function. The response of the global model in the Northern Hemisphere is then used to initialize the hemispheric models.

Since the global model is initialized with a linear model, one must expect that for certain zonal winds certain preferred resonant waves will dominate. As mentioned previously, if the zonal streamfunction is close to a particular resonance value then the dominant waves in the model should be the resonant waves, and these waves will be almost stationary in the global model (see also Tung and Lindzen, 1979). This does not mean that all other waves are absent. Other waves are also present, but their amplitudes are very small compared to those of the resonant waves and hence they are usually relatively unimportant for short-term forecasts. However, in the hemispheric models, these waves may not be small, especially if the global resonant wave does not appear in the truncated spectrum available to the hemispheric model. In that case the hemispheric model must use the available spectrum to describe the initial state. The waves in this hemispheric spectrum will not be near a resonance point and will have anomalous propagation speeds. That is to say, if a hemispheric model does not contain the global wave then we expect a very poor representation of the subsequent evolution of the system. As we shall see, for the largest wavelengths this error becomes noticeable almost immediately.

Thus, certain waves can be selectively excited by choosing the zonal wind appropriately. This was done by examining Fig. 1a to determine the value of the zonal wind that was likely to give a large response in a particular wave. In this way we chose cases for which the symmetric model would perform better than the antisymmetric model and cases for which the symmetric model would be worse than the antisymmetric model. For example, case 4 preferen-

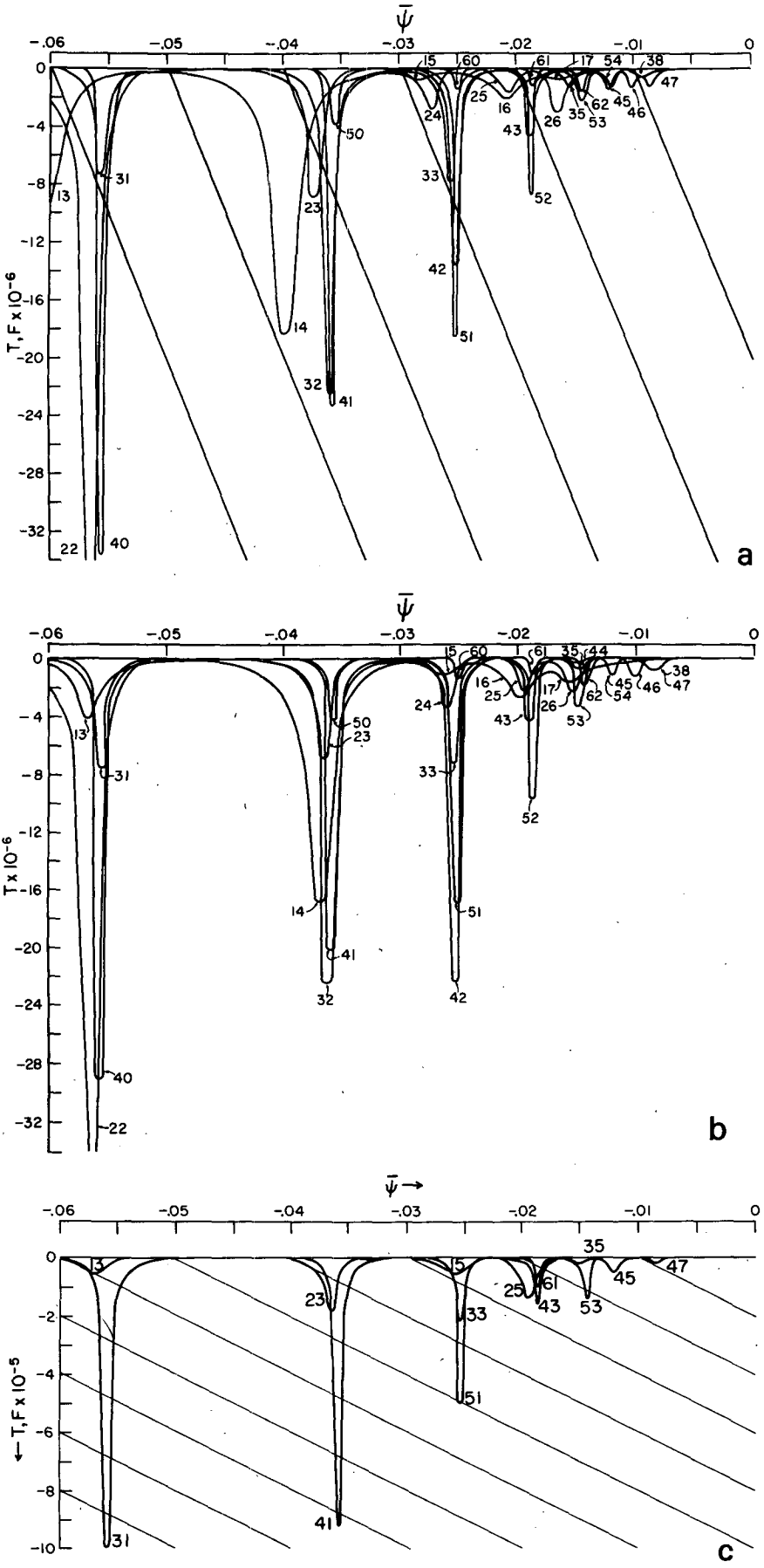

TABLE 2. Period in days for wave 3. Periods for other waves can be found by multiplying by 3 $m^{-1}$, where $m$ is the zonal wavenumber. The values are irrelevant for $m > n$. Positive values indicate westward propagating waves and negative values indicate eastward propagating waves.

| $n$ | $\bar{\psi}$ | 1 | 2 | 3 | 4 | 5 | 6 | 7 | 8 | 9 | 10 |
|---|---|---|---|---|---|---|---|---|---|---|---|
| 2 | −0.25 | 0.33 | ∞ | −1.3 | −0.95 | −0.83 | −0.78 | −0.75 | −0.73 | −0.71 | −0.70 |
| 3 | −0.1 | 0.33 | 1.7 | ∞ | −4.2 | −2.8 | −2.3 | −2.1 | 2.0 | −1.9 | −1.9 |
| 4 | −0.0556 | 0.33 | 1.3 | 4.5 | ∞ | −8.9 | −5.7 | −4.6 | −4.1 | −3.8 | −3.7 |
| 5 | −0.0357 | 0.33 | 1.2 | 3.1 | 9.3 | ∞ | −16 | −10 | −8.0 | −7.0 | −6.4 |
| 6 | −0.0250 | 0.33 | 1.1 | 2.7 | 6.0 | 17 | ∞ | −27 | −16 | −12.5 | −11 |
| 7 | −0.0185 | 0.33 | 1.1 | 2.4 | 5.0 | 10 | 27 | ∞ | −41 | −24 | −17 |
| 8 | −0.0143 | 0.33 | 1.1 | 2.3 | 4.5 | 8.3 | 16 | 41 | ∞ | −58 | −34 |
| 9 | −0.0114 | 0.33 | 1.0 | 2.3 | 4.2 | 7.3 | 13 | 24 | 59 | ∞ | −79 |
| 10 | −0.00926 | 0.33 | 1.0 | 2.2 | 4.0 | 6.7 | 11 | 19 | 34 | 81 | ∞ |

tially excites resonant wave 42, and the symmetric model should work better than the symmetric model for this case. Case 3 preferentially excites resonant wave 33, and the better prediction is likely to be that of the antisymmetric model. Case 2 does not preferentially excite any resonant wave and thus both models are likely to be bad, but the symmetric model should be worse initially simply because its waves have the smallest period. Case 1 preferentially excites resonant wave 14, and the symmetric model should be better for this case.

Fig. 2 shows the trough-ridge diagrams associated with the four cases. Here the wave as a function of time is shown in the global model, and the anomalous waves in the hemispheric model (the differences between the actual wave and the global model wave) are also shown as a function of time. Note that the anomalous waves have the largest phase speeds for the smallest wavenumbers. It is also clear that the symmetric model is best for case 4, the antisymmetric model is best for case 3 and that neither model does very well for case 2. Because of its larger phase speeds, the symmetric model is actually worse than the antisymmetric model for case 2. The final case for wavenumber 1 shows that the worst results occur for the antisymmetric model, although the symmetric model, because of its small periods and improper initialization of the stationary wave, is not much better.

### *b. Other zonal flows and propagating wave initialization*

We next examine the time-dependent responses for zonal flows with a more realistic structure than solid body rotation. Consider the two basic structures shown in Fig. 3. Case *C* refers to the case with tropical easterlies and critical lines separating westerlies from easterlies, and case *N* refers to the case with tropical westerlies and no critical lines. These two cases illustrate how small changes in the tropical wind structure can affect the solutions.

The linear solution for zonal wavenumber 1 for these two zonal wind structures is shown in Fig. 4a. Note the close similarity between the solutions with and without tropical easterlies, which indicates that for this case the tropical winds have only a small influence upon the resulting solutions. This is not the case, however, when the winds are increased by an arbitrary factor of 5, not an unreasonable value in the context of linear barotropic theory. As shown in Fig. 4b, distinct differences now appear between the cases with and without tropical easterlies. Presumably these differences occur because the larger zonal wind excites a Rossby wave of larger meridional wavelength, and this wave is excited preferentially near the South Pole. The presence or absence of the critical line and tropical easterlies then affects the meridional propagation differently, resulting in substantially different solutions in the Northern Hemisphere, as can be seen clearly in Fig. 4b. The linear solution for zonal wavenumber two, shown in Fig. 4c, shows that this wave is preferentially excited in the Northern Hemisphere and that again the presence or absence of the tropical easterlies can have a large influence upon the resulting solutions.

We next consider time-dependent integrations of the zonally asymmetric equations initialized with the stationary solutions discussed above. We shall con-

FIG. 1. (a) The stationary solutions in the global model. The straight lines depict the frictional forcing and dissipation as a function of the zonal streamfunction, $\bar{\psi}_1$. The different lines are for different values of $\bar{\psi}_e$, the forcing equilibrium, which is the zero-intercept of the straight lines. The spectra-like curves are the mountain torque as a function of $\bar{\psi}$. The zonal streamfunction increases from large negative values to zero and the values are in nondimensional units. The resonant peaks are labeled by the wavenumber and by the number of zeros in the meridional function between the poles, with the same code as in Table 1. (b) As in (a) except $gh = 0$ and the friction function is not shown. (c) As in (a) except for the antisymmetric hemispheric model. Note that the scale of the ordinate differs from that of (a) and (b).

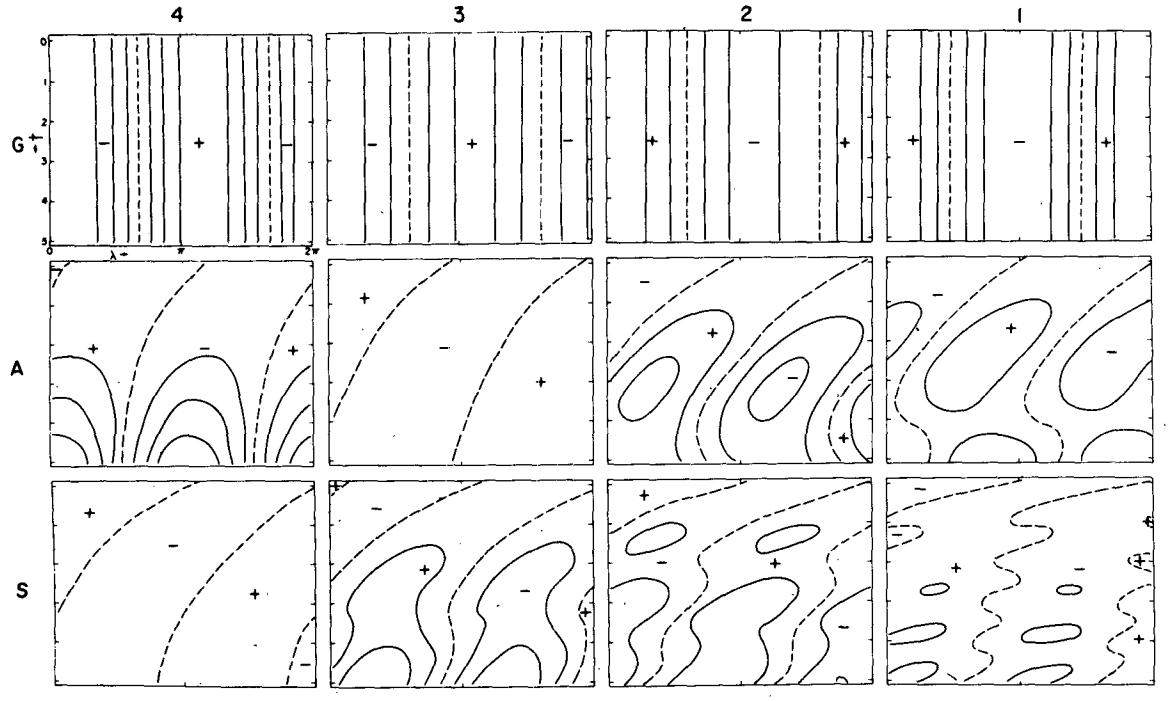


FIG. 2. Trough–ridge diagrams for four case studies with global and hemispheric models in solid-body rotation. The global models are denoted by the letter *G* and the antisymmetric and symmetric hemispheric models are denoted by the letters *A* and *S*, respectively. The four case studies denoted by numbers 4, 3, 2, 1, refer to the wavenumber used in the experiments described in the text. In each trough–ridge diagram, time runs downward in days and the horizontal coordinate is longitude ranging over one wavelength of each wave. The streamfunction at 40°N is contoured every $10^{-3}$ nondimensional units for cases 1, 3 and 4, and every $10^{-4}$ nondimensional units for case 2. The total streamfunction is given for the global models and the anomalous streamfunction is given for the hemispheric models.

sider eight time-dependent cases. The first four cases deal with stationary wave initialization of zonal wavenumber 1 and are shown in Fig. 5. Because the zonal flow was arbitrarily selected without regard to preferred wave responses, we might expect that both hemispheric models would show considerable error. However, both models display relatively little error, <10%, at least within the five days of the integration. It is noteworthy that this result occurs regardless of whether or not tropical easterlies are present. Presumably, this relatively accurate solution was obtained because the aliased initial projection of the global modes onto the largest hemispheric modes was small. Thus, in spite of the fast phase speeds of these modes, their small initial amplitudes prevent them from causing large errors within the 5-day integration period.

A substantially different result occurs, however, when the zonal wind is increased by a factor of 5. Here the lowest modes have a large initial projection and lead to large errors in the hemispheric models. Note that this error field is large in both the models (1*C*5 with and 1*N*5 without tropical easterlies), suggesting that an especially important factor is how the initial state is projected onto the lowest-order modes which have the fastest phase speeds.

As a final example of this phenomenon, we consider a propagating wave initialization. For this case, the zonal wind of Fig. 3, increased by a factor of 5,

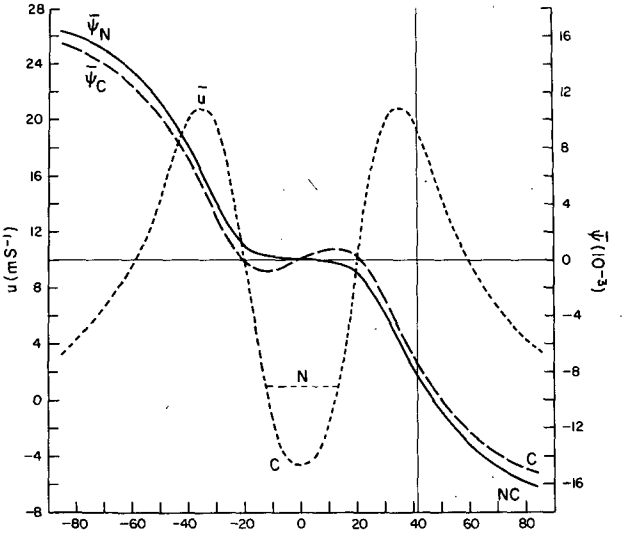


FIG. 3. The zonal flows and associated streamfunctions, adapted from Oort and Rasmussen (1971). *C* refers to the zonal flow with critical lines, and *N* refers to the zonal flow without critical lines.

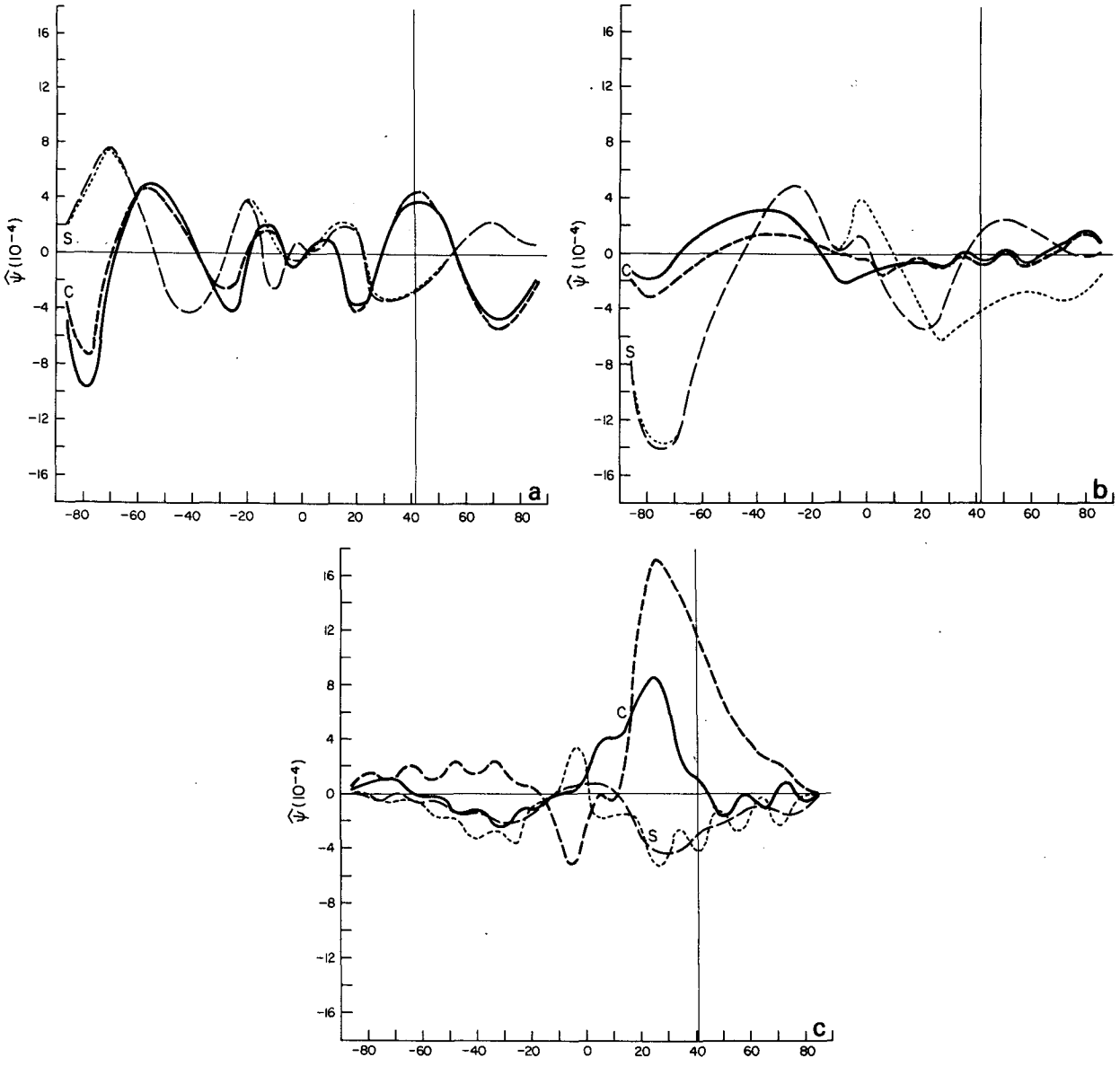


FIG. 4. (a) The meridional structure of the asymmetric streamfunction for zonal wavenumber 1, found from the global linear model, and the case in which the zonal flow is that shown in Fig. 3. The thick lines ($C$) show the cosine component as a function of latitude. Here the solid line is for the case with tropical easterlies and the dashed line is for the case with tropical westerlies. The thin lines ($S$) show the sine component. Here the case with tropical easterlies is shown in long dashes, and short dashes represent the case with tropical westerlies. (b) As in (a) except for the case in which the zonal flow is 5 times the profile shown in Fig. 3. Comparison of (a) and (b) shows that the presence or absence of a critical line is very significant for the case with the stronger zonal flow. (c) As in (b) except for zonal wavenumber 2.

was used to find the linear stationary state. Then the zonal wind reduced to its original value was employed as the constant zonal state throughout the integration. In this case, the asymmetric state is not in balance with the zonal state of the global model and the trough–ridge diagrams for the global model show a westward phase progression (Fig. 6). For cases with zonal wavenumbers 1 and 2, both with and without critical lines, the error projections onto the lowest hemispheric modes are large, and substantial errors appear within 5 days. As can be seen in Fig. 6, the magnitudes of these errors shown for the antisymmetric ($A$) and symmetric ($S$) hemispheric solutions are comparable to the magnitude of the global ($G$) solutions themselves.

## 5. Conclusions

A global, quasi-linear, quasi-geostrophic barotropic model forced by orography and a zonal forcing

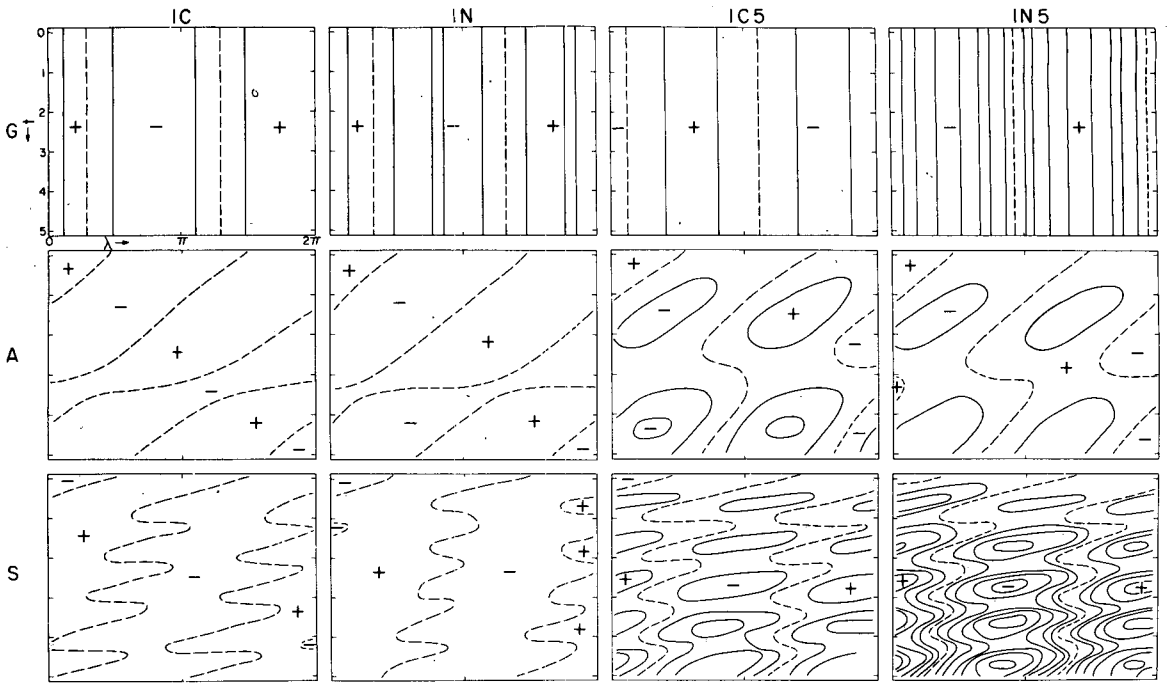


FIG. 5. As in Fig. 2, except 1*C* refers to the case using zonal wavenumber 1 and the zonal flow with tropical easterlies, and 1*N* refers to the case using wavenumber 1 and the zonal flow with tropical westerlies. 1*C*5 and 1*N*5 use the same zonal flow structure as 1*C* and 1*N* but have the winds multiplied by a factor of 5. For each of the four cases, the error field shown for the asymmetric (*A*) and symmetric (*S*) models has the same contour interval as the solution of the corresponding global (*G*) model.

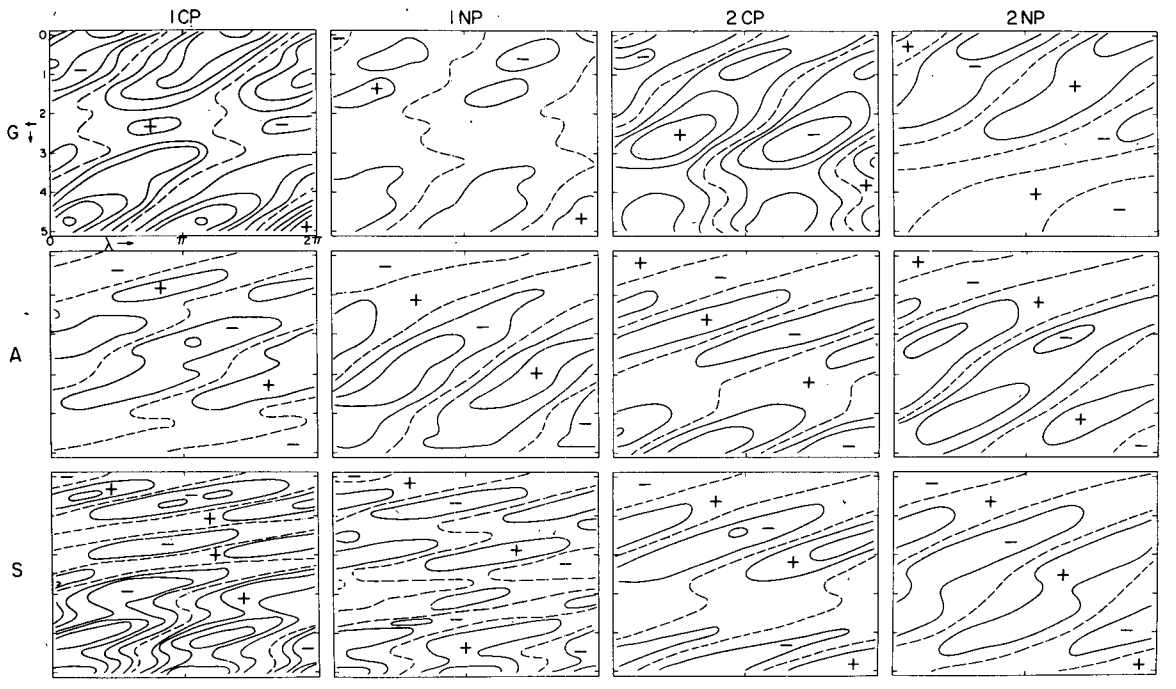


FIG. 6. As in Fig. 5, except that the initial solution is a westward propagating wave. 1*CP* and 1*NP* refer to the cases using wavenumber 1, and 2*CP* and 2*NP* refer to the cases using zonal wavenumber 2. Again *C* denotes cases with critical lines (tropical easterlies), and *N* denotes cases without critical lines (tropical westerlies).

and dissipated by friction has been compared to two hemispheric models, one with antisymmetric equatorial boundary conditions and one with symmetric equatorial boundary conditions.

The stationary solutions in these models were found to be different, because the hemispheric models lacked either the symmetric or the antisymmetric waves, and because the mountain torque was much larger in the hemispheric models. Naturally, this conclusion, drawn from a quasi-linear model, is not necessarily true for the fully nonlinear case.

A comparison of 5-day integrations showed that a crucial factor in determining whether symmetric or antisymmetric hemispheric models could be used for short-term forecasts was whether symmetric or antisymmetric waves were excited in the global model. If the initial conditions contained only antisymmetric or symmetric waves, one could choose the corresponding hemispheric model. For the mixed case, however, a global model is necessary.

Because of the known sensitivity of the meridional propagation of Rossby waves to the presence or absence of critical lines (Dickinson, 1968), one might anticipate that the ability of a hemispheric model to reproduce the solution of a global model would also depend strongly on whether critical lines were present. We found that the critical lines can be important in determining the stationary solution. However, our results suggest that in determining whether or not hemispheric models can be used for short-term forecasts, the crucial factor is the projection of the initial conditions onto the gravest modes, which have the fastest phase speeds. If the projection is small, then either hemispheric model can be used for short-term forecasts. If the projection is large and incorrect, then the hemispheric models will yield erroneous predictions, whether or not critical lines are present.

These results are largely consistent with those of an independent analysis (Daley *et al.*, 1981), focused on one of the cases of Somerville (1980). The study of Daley *et al.* also confirms the predominantly linear and barotropic character of the error, as discussed by Lambert and Merilees (1978).

The processes which produce spurious Rossby waves in our simple hemispheric models may also act in more complicated models. We therefore conclude that, although there will be cases for which hemispheric models will make forecasts almost as skillful as those of a global model, in general, global models are preferable.

*Acknowledgments.* The research of J. O. Roads was supported by NASA grant G-NAG5-105. We are grateful for helpful comments from W. Baker, J. Tribbia and G. Vallis. We especially thank G. Johnston for typing various versions of the manuscript and F. Crowe for drafting the figures. We are also grateful for the comments by the anonymous reviewers.

## REFERENCES

Baer, F., and G. W. Platzman, 1961: A procedure for numerical integration of the spectral vorticity equation. *J. Meteor.*, **19,** 393–401.

Baumhefner, D. P., 1971: On the effects of an imposed southern boundary on numerical weather prediction in the Northern Hemisphere. *J. Atmos. Sci.*, **28,** 42–54.

Charney, J. G., and J. G. Devore, 1979: Multiple flow equilibria in the atmosphere and blocking. *J. Atmos. Sci.*, **36,** 1205–1216.

Daley, R., J. Tribbia and D. L. Williamson, 1981: The excitation of large-scale free Rossby waves in numerical weather prediction. *Mon. Wea. Rev.*, **109,** 1836–1861.

Dickinson, R. E., 1968: Planetary Rossby waves propagating vertically through weak westerly wind wave guides. *J. Atmos. Sci.*, **25,** 984–1002.

Lambert, S. J., and P. E. Merilees, 1978: A study of planetary wave errors in a spectral numerical weather prediction model. *Atmos. Ocean.*, **16,** 197–211.

Lorenz, E. N., 1960: Energy and numerical weather prediction. *Tellus*, **12,** 364–373.

Miyakoda, K., and Umscheid, L., Jr., 1973: Effects of an equatorial "wall" on an atmospheric model. *Mon. Wea. Rev.*, **101,** 603–616.

Oort, A. H., and E. M. Rasmusson, 1971: *Atmospheric Circulation Statistics.* NOAA Prof. Pap. No. 5, 323 pp.

Roads, J. O., 1980a: Stable near-resonant states forced by perturbation heating in a simple baroclinic model. *J. Atmos. Sci.*, **37,** 1957–1967.

——, 1980b: Stable near-resonant states forced by orography in a simple baroclinic model. *J. Atmos. Sci.*, **37,** 2381–2395.

——, 1981: Quasi-linear blocks forced by orography in a hemispheric quasi-geostrophic barotropic model. *Mon. Wea. Rev.*, **109,** 1421–1437.

Somerville, R. C. J., 1980: Tropical influences on the predictability of ultralong waves. *J. Atmos. Sci.*, **37,** 1141–1156.

Tung, K. K., and R. S. Lindzen, 1979: A theory of stationary long waves. Part I: A simple theory of blocking. *Mon. Wea. Rev.*, **107,** 714–734.